



HAL
open science

Relation between the weak itinerant magnetism in A_2Ni_7 compounds ($A = Y, La$) and their stacked crystal structures

J-C Crivello, V. Paul-Boncour

► **To cite this version:**

J-C Crivello, V. Paul-Boncour. Relation between the weak itinerant magnetism in A_2Ni_7 compounds ($A = Y, La$) and their stacked crystal structures. *Journal of Physics: Condensed Matter*, 2020, 32 (14), pp.145802. 10.1088/1361-648x/ab6045 . hal-02436487

HAL Id: hal-02436487

<https://hal.science/hal-02436487>

Submitted on 1 Oct 2020

HAL is a multi-disciplinary open access archive for the deposit and dissemination of scientific research documents, whether they are published or not. The documents may come from teaching and research institutions in France or abroad, or from public or private research centers.

L'archive ouverte pluridisciplinaire **HAL**, est destinée au dépôt et à la diffusion de documents scientifiques de niveau recherche, publiés ou non, émanant des établissements d'enseignement et de recherche français ou étrangers, des laboratoires publics ou privés.

Relation between the weak itinerant magnetism in A_2Ni_7 compounds ($A = Y, La$) and their stacked crystal structures

J-C Crivello[✉] and V Paul-Boncour[✉]

Univ. Paris Est Creteil, CNRS, ICMPE, UMR7182, F-94320 Thiais, France

E-mail: paulbon@icmpe.cnrs.fr

Received 15 April 2019, revised 22 November 2019

Accepted for publication 10 December 2019

Published 7 January 2020



Abstract

The weak itinerant magnetic properties of A_2Ni_7 compounds with $A = \{Y, La\}$ have been investigated using electronic band structure calculations in the relation with their polymorphic crystal structures. These compounds crystallize in two structures resulting from the stacking of two and three blocks of $[A_2Ni_4 + 2 ANi_5]$ units for hexagonal $2H-La_2Ni_7$ (Ce_2Ni_7 type) and rhombohedral $3R-Y_2Ni_7$ (Gd_2Co_7 type) respectively. Experimentally, $2H-La_2Ni_7$ is a weak itinerant antiferromagnet whereas $3R-Y_2Ni_7$ is a weak itinerant ferromagnet. From the present first principles calculation within non-spin polarized state, both compounds present an electronic density of state with a sharp and narrow peak centered at the Fermi level corresponding to flat bands from $3d-Ni$. This induces a magnetic instability and both compounds are more stable in a ferromagnetic (FM) order compared to a paramagnetic state ($\Delta E \approx -35$ meV/f.u.). The magnetic moment of each of the five Ni sites varies with their positions relative to the $[A_2Ni_4]$ and $[ANi_5]$ units: they are minimum in the $[A_2Ni_4]$ unit and maximum at the interface between two $[ANi_5]$ units. For $2H-La_2Ni_7$, an antiferromagnetic (AFM) structure has been proposed and found with an energy comparable to that of the FM state. This AFM structure is described by two FM unit blocks of opposite Ni spin sign separated by a non-magnetic layer at $z = 0$ and $\frac{1}{2}$. The Ni ($2a$) atoms belonging to this intermediate layer are located in the $[La_2Ni_4]$ unit and are at a center of symmetry of the hexagonal cell ($P6_3/mmc$) where the resultant molecular field is cancelled. Further non-collinear spin calculations have been performed to determine the Ni moment orientations which are found preferentially parallel to the c axis for both FM and AFM structures.

Keywords: intermetallic, electronic structure, weak itinerant magnetism, antiferromagnetism, first principle calculation

 Supplementary material for this article is available [online](#)

(Some figures may appear in colour only in the online journal)

1. Introduction

Weak itinerant ferromagnets (wFM) and antiferromagnets (wAFM) are not very common and have raised a large and ongoing interest as they are near the onset of magnetism, present large spin-fluctuations and are often close to quantum critical point and even superconductivity [1–3]. Among the wFM, several studies have been performed on $ZrZn_2$ [4, 5],

Ni_3Al [6–10], Fe_2N [11, 12] and $AsNCr_3$ [13]. wAFM are even less common than wFM and have been observed in some compounds like $TiBe_2$ [14–16], $TiAu$ [17–20] and UN [21]. Weak itinerant magnets are generally characterized by high transition temperatures and low magnetic moments related to their particular electronic properties.

Recently Singh [22] has compared wFM classical face-centered-cubic Ni substituted by Al forming the Ni_3Al (75%

Ni) with wFM Y_2Ni_7 which is also a Ni rich compound (78% Ni). Y_2Ni_7 is an interesting itinerant magnet which has deserved both detailed theoretical and experimental studies [23–25].

With the same stoichiometry than Y_2Ni_7 , La_2Ni_7 has been the subject of many experimental studies revealing a weak itinerant antiferromagnetic ground state, whose origin has not been clearly solved until now. Due to the very few number of wAFM compounds, it appears of particular interest to describe the AFM structure of La_2Ni_7 and to understand the origin of its specific behavior.

La_2Ni_7 crystallizes preferentially in the hexagonal Ce_2Ni_7 structure type and Y_2Ni_7 in the rhombohedral Gd_2Co_7 structure type. Hexagonal La_2Ni_7 is a wAFM with $T_N = 50$ K and undergoes a metamagnetic transition toward a wFM state [26–30], whereas rhombohedral Y_2Ni_7 is a wFM with $T_C = 53$ K [22, 23, 25, 31, 32]. Both compounds have in common low value of the mean Ni moments (0.06 to 0.11 μ_B/Ni) [25, 30] and relatively large ordering temperatures, characteristic of the weak itinerant magnetism. They have also effective Ni moments around $\mu_{eff} = 0.8–1 \mu_B$ and positive paramagnetic Curie temperatures θ_p between 50 and 70 K derived from the analysis of their magnetic susceptibility in the paramagnetic range [23, 25, 27, 30]. This is rather surprising for La_2Ni_7 , as a negative θ_p is expected for an antiferromagnetic compound.

Several experimental studies have confirmed the wAFM behavior of La_2Ni_7 at low field, but the attempts to perform neutron powder diffraction (NPD) experiments at low temperature [33] did not allow to determine its microscopic magnetic structure. The absence of magnetic peaks in the neutron patterns below T_N was attributed to the itinerant character of the antiferromagnetism and the low values of the Ni moments.

In order to solve the origin of the weak antiferromagnetic ground state of La_2Ni_7 as well as its metamagnetic transition toward a ferromagnetic structure, we have performed first principle calculations using collinear and non-collinear spin polarized density-functional theory (DFT). Taking into account the particular geometry of the La_2Ni_7 crystal structure, we will propose an antiferromagnetic structure which can explain, for the first time, many of the magnetic experimental particularities of this compound.

The magnetic and electronic properties of La_2Ni_7 will be compared with those of Y_2Ni_7 all along this paper. A more general discussion on the specific itinerant magnetic behavior of La_2Ni_7 compared to other intermetallic compounds with large spin fluctuations will be introduced.

2. Structural description and methodology

La_2Ni_7 and Y_2Ni_7 crystallize in a Ce_2Ni_7 type hexagonal structure ($P6_3/mmc$ space group) and Gd_2Co_7 -type rhombohedral structure (trigonal symmetry, $R\bar{3}m$ space group) respectively as presented in figure 1. These phases result from the stacking of $[A_2B_4]$ and $[AB_5]$ units according to the rule $[A_2B_4 + n \cdot AB_5]$, where n is an integer. If $n = 2$, the stacking leads to the A_2B_7 formation in two polymorphic forms: the hexagonal Ce_2Ni_7 cell [2H] contains two blocks of $[A_2B_4 + 2 AB_5]$,

whereas the rhombohedral Gd_2Co_7 cell [3R] contains three blocks of $[A_2B_4 + 2 AB_5]$ in the hexagonal description as shown in figure 1 [34]. For the sake of simplicity, the $[A_2B_4]$ subunit will be renamed as $[AB_2]$ in the following. Both hexagonal and rhombohedral structures are strongly anisotropic, with large values of the c parameter compared to the a parameter ($a = 5.062 \text{ \AA}$, $c = 24.71 \text{ \AA}$ for 2H- La_2Ni_7 ; $a = 4.946 \text{ \AA}$ and $c = 36.26 \text{ \AA}$ for 3R- Y_2Ni_7). Both cell contains $2 A = \{Y, La\}$ and $5 B = Ni$ different Wyckoff sites (table 1) which are characterized by their positions along the c axis forming A and Ni layers. Each A site is located either in one $[AB_5]$ or one $[AB_2]$ units, whereas each Ni site is located either in one of these units or at the interface between 2 units. Regarding the Ce_2Ni_7 type structure, it displays a mirror inversion of the $[AB_2]$ units at $z = 0$ and $z = 1/2$.

The electronic structure was calculated for the ordered La_2Ni_7 and Y_2Ni_7 compounds in both hexagonal and rhombohedral structures. In the frame of the DFT, the pseudo-potential approach using the VASP package [35, 36] was considered using projector-augmented wave [37] with a 600 eV cut-off energy and a high k -mesh density (at least 250 k -point in the irreducible Brillouin zone). Several exchange and correlation (XC) functionals have been considered, such as local density approximation (LDA) with parametrization from Perdew and Zunger [38], the generalized gradient approximation with the PBE functional [39, 40] and a meta-GGA functional, the strongly constrained and appropriately normed semi-local density functional (SCAN) [41], including the second derivative of the electron density. In addition, an empirical coulomb interaction (Hubbard) was introduced ($U = 5$ eV, $J = 0$) to test the influence of GGA + U calculation [42]. Preserving the original crystal symmetry, each structure has been fully relaxed within several magnetic ordering such as ferromagnetic and antiferromagnetic structure using the electronic collinear and non-collinear spin-polarization. For the latter, the most stable spin moments orientation has been investigated in GGA-PBE (several moment directions have been tested such as parallel and perpendicular to c axis). Final static calculation was done using the linear tetrahedron method with Blöchl corrections on relaxed structures [43]. The charge distribution on the atoms was investigated using Bader topological analysis within the ‘Bader’ code developed by Henkelman *et al* [44, 45].

3. Results and discussion

The non-spin polarized (NSP) density of state (DOS) of hexagonal La_2Ni_7 (2H- La_2Ni_7) and rhombohedral Y_2Ni_7 (3R- Y_2Ni_7) are compared in figure 2(left). The electronic DOS results in a large main structure dominated by the $3d$ states from Ni. A charge transfer from the A element to Ni is observed (1.2 e-per A atom according to the Bader method), but is not sufficient to completely fill the Ni-bands and both compounds present a DOS with a sharp and narrow peak centered at the Fermi level (E_F). This result is in agreement with previous studies [22, 46, 47] and was also observed in wAFM orthorhombic TiAu [18, 19] and H_3S superconductor [48]. This peak corresponds to the

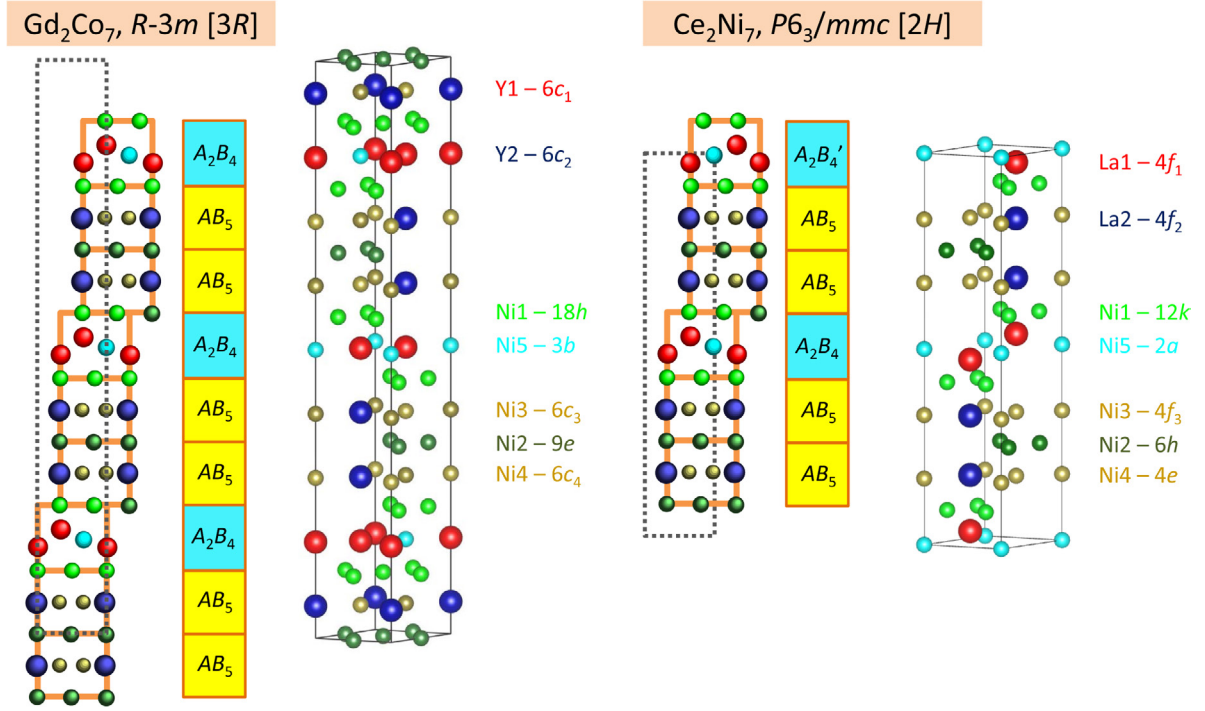


Figure 1. Comparison of the rhombohedral and hexagonal structures of A_2Ni_7 compounds showing the stacking of $[AB_2]$ and $[AB_5]$ units and the A and Ni atom positions.

Table 1. Calculated magnetic moments in hexagonal La_2Ni_7 (FM, AFM) and rhombohedral Y_2Ni_7 (FM). $\Delta E = E - E_0$ (NSP).

$2H-La_2Ni_7$				FM	AFM
Atom	Site	Unit	Neighbors	m ($\mu_B/at.$)	m ($\mu_B/at.$)
La1	$4f_1$	$[AB_2]$	4 A + 12 Ni	-0.026	± 0.015
La2	$4f_2$	$[AB_5]$	2 A + 18 Ni	-0.041	± 0.041
Ni1	$12k$	$[AB_2/AB_5]$	5 A + 7 Ni	0.102	± 0.095
Ni2	$6h$	$[AB_5]$	4 A + 8 Ni	0.287	± 0.293
Ni3	$4f_3$	$[AB_5]$	3 A + 9 Ni	0.198	± 0.186
Ni4	$4e$	$[AB_5]$	3 A + 9 Ni	0.197	± 0.197
Ni5	$2a$	$[AB_2]$	6 A + 6 Ni	0.023	0
M_{total} ($\mu_B/f.u.$)				1.08	0
ΔE (eV/f.u.)				-0.035	-0.033
$3R-Y_2Ni_7$				FM	
Atom	Site	Unit	Neighbors	m ($\mu_B/at.$)	
Y1	$6c_1$	$[AB_5]$	2 A + 18 Ni	-0.043	
Y2	$6c_2$	$[AB_2]$	4 A + 12 Ni	-0.034	
Ni1	$18h$	$[AB_2/AB_5]$	5 A + 7 Ni	0.153	
Ni2	$9e$	$[AB_5]$	4 A + 8 Ni	0.315	
Ni3	$6c_3$	$[AB_5]$	3 A + 9 Ni	0.208	
Ni4	$6c_4$	$[AB_5]$	3 A + 9 Ni	0.216	
Ni5	$3b$	$[AB_2]$	6 A + 6 Ni	0.071	
M_{total} ($\mu_B/f.u.$)				1.238	
ΔE (eV/f.u.)				-0.035	

flat d -bands in the electronic band structure as shown in figures 2(right, zoom scale) and S1(full scale) (stacks.iop.org/JPhysCM/32/145802/mmedia) for $2H-La_2Ni_7$. Such flat bands were also visible for the paramagnetic calculation of $3R-Y_2Ni_7$ in [22]. It can be noticed that the peak maximum is located at E_F for Y_2Ni_7 , while it is slightly shifted to higher energy for

La_2Ni_7 . The main contribution to this peak is thus due to the $3d$ states of Ni and leads to a high DOS at E_F ; $N(E_F) = 14.6$ states/eV per f.u. for $2H-La_2Ni_7$, smaller than that calculated for $3R-Y_2Ni_7$: $N(E_F) = 21.7$ states/eV per f.u. (close to the 24 states/eV per f.u. from [22]). Both values are large enough to follow the Stoner criterion [49] ($N(E_F) * I > 1$ for $I \approx 0.8$

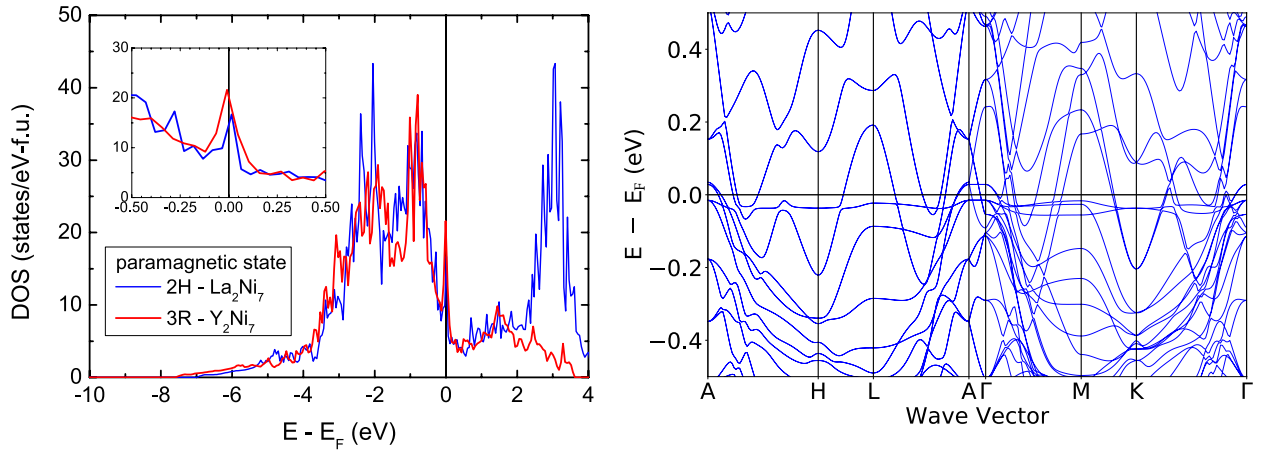


Figure 2. Non-spin polarized density of state of $3R\text{-Y}_2\text{Ni}_7$ and $2H\text{-La}_2\text{Ni}_7$ with a zoom near E_F in the inset (left) and corresponding electronic band structure of $2H\text{-La}_2\text{Ni}_7$ zoomed near E_F (right) in GGA-PBE. The full scale of the latter is given in supplementary materials.

eV/at usually taken for transition metals) and induce a lowering of the total energy by a shift of the minority and majority bands.

The calculated spin polarized DOS of $3R\text{-Y}_2\text{Ni}_7$ and $2H\text{-La}_2\text{Ni}_7$, assuming a ferromagnetic ground state, are displayed in figures 3(a) and (b) respectively. The calculated moments for each atomic site as well as the magnetic energies (ΔE) are reported in table 1. The high density peak position is shifted to lower and higher energy for spin up and spin down bands respectively and $N(E_F)$ decreases due to its position located in a valley of the density of states. As a consequence the total energy of ferromagnetic state is lowered by 5 meV/Ni atom compared to NSP calculated value for both compounds. This magnetic energy corresponds to a temperature of 58 K, which is close to the experimental ordering temperature of Y_2Ni_7 ($T_C = 53$ K) [25].

The calculated moment for each atomic site in ferromagnetic state are reported in table 1. The magnetic moments in Y_2Ni_7 are in good agreement with those calculated by Singh using a linear augmented plane-wave method [22]. It is noticeable, that the total calculated moments of $1.08 \mu_B/\text{f.u.}$ for La_2Ni_7 and $1.24 \mu_B$ for Y_2Ni_7 are larger than experimental values ($0.77 \mu_B/\text{f.u.}$ and $0.43 \mu_B/\text{f.u.}$ measured at 4.2 K and extrapolated from high field for $A = \text{La}$ and Y respectively) [25, 27]. This overestimation is due to the limit of our DFT calculations, which do not take into account the large spin fluctuations present in such compounds. The Ni moments contribute mainly to the total magnetization, whereas the induced A moments remain weak and are, as expected, of opposite sign compared to Ni moments.

Further non-collinear spin calculations have been performed to determine the preferential orientation of the Ni moments in the FM structure. The Ni moments are stabilized in the direction parallel to the c axis: the energy difference between moments parallel and perpendicular to the c axis is about -30 meV/f.u..

The coordination polyhedra have been represented with their calculated magnetic vectors for the Ni1 to Ni4 sites in figure 4 and for the Ni5 site in figure 5(right) for hexagonal La_2Ni_7 in the ferromagnetic state. In a first approximation, the

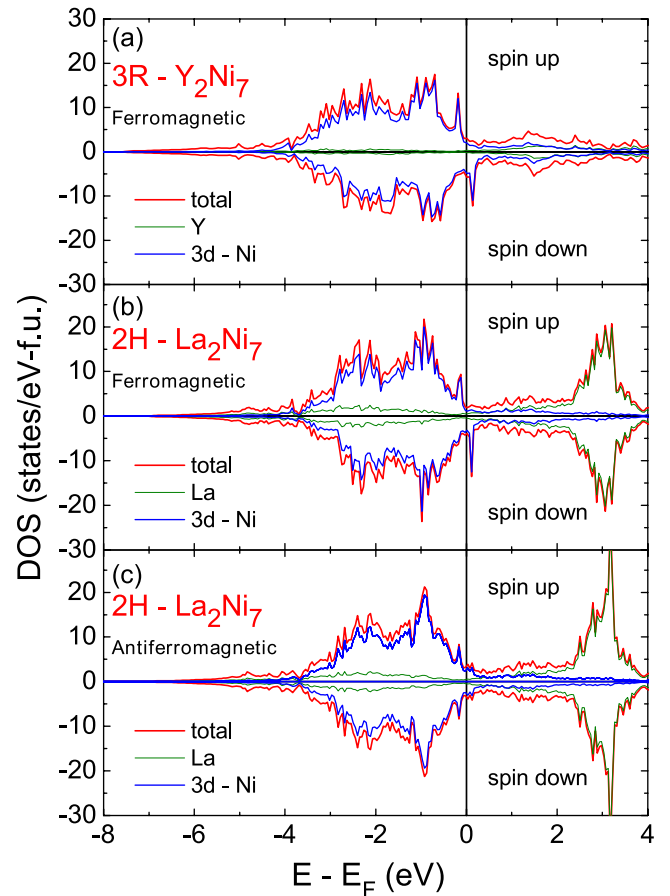


Figure 3. Calculated spin polarized DOS with partial $3d\text{-Ni}$ contribution for (a) ferromagnetic $3R\text{-Y}_2\text{Ni}_7$ ($M = 1.24 \mu_B/\text{f.u.}$), (b) ferromagnetic $2H\text{-La}_2\text{Ni}_7$ ($M = 1.08 \mu_B/\text{f.u.}$) and (c) antiferromagnetic $2H\text{-La}_2\text{Ni}_7$ ($M = 0 \mu_B/\text{f.u.}$).

magnitude of Ni moments should depend on the number of Ni neighbors and of the site symmetry. Assuming that the Ni moments should be larger for atoms surrounded by a larger number of Ni neighbors, the Ni3 and Ni4 atoms, which have similar coordination environment with 9 Ni neighbors and 3 A neighbors, are expected to have larger magnetic moments

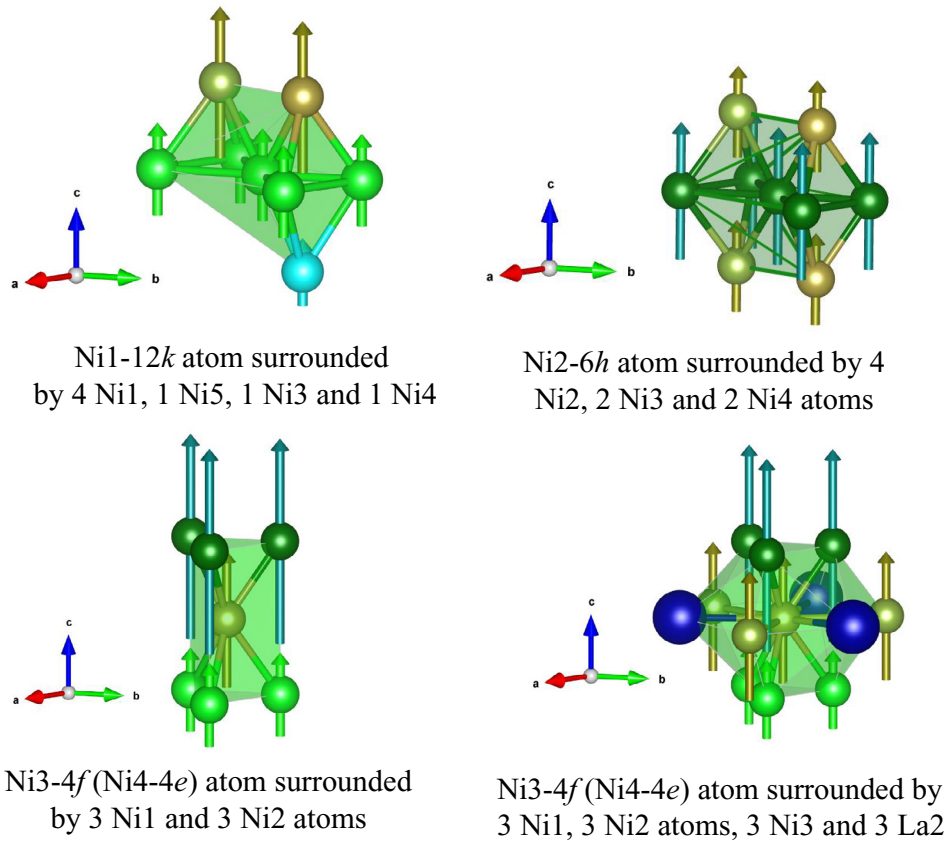


Figure 4. Coordination polyhedra around the Ni1, Ni2 and Ni3 (Ni4) atoms. For the Ni3 (Ni4) atoms two types of polyhedra have been represented for interatomic distances below 2.65 Å (left) and below 2.95 Å (right) The magnetic vectors have been represented with length proportional to their magnetic moments.

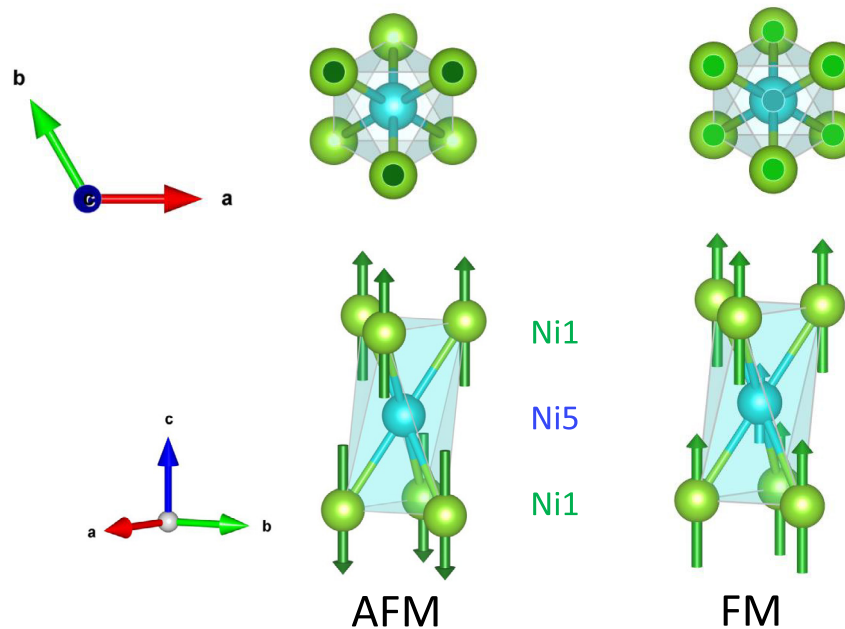


Figure 5. Coordination polyhedra of Ni5 atoms surrounded by Ni1 atoms with magnetic vectors in AFM and FM ordering perpendicular (top) and parallel (bottom) to the *c* axis.

than the Ni2 atom surrounded by only 8 Ni neighbors, but the calculation indicates that the Ni2 moment is the largest (table 1). In fact, a closer analysis of the Ni–Ni pair distances shows that each Ni3 (Ni4) atom is surrounded by three Ni2 at

$2.45 \pm 0.5 \text{ \AA}$, three Ni1 at $2.52 \pm 0.5 \text{ \AA}$ and three Ni4 (Ni3) atoms distant of $2.92 \pm 0.5 \text{ \AA}$ (at the same distance than the 3 *A* neighbors). The larger Ni4–Ni3 distance corresponds to weaker Ni–Ni bonds and smaller exchange interaction with

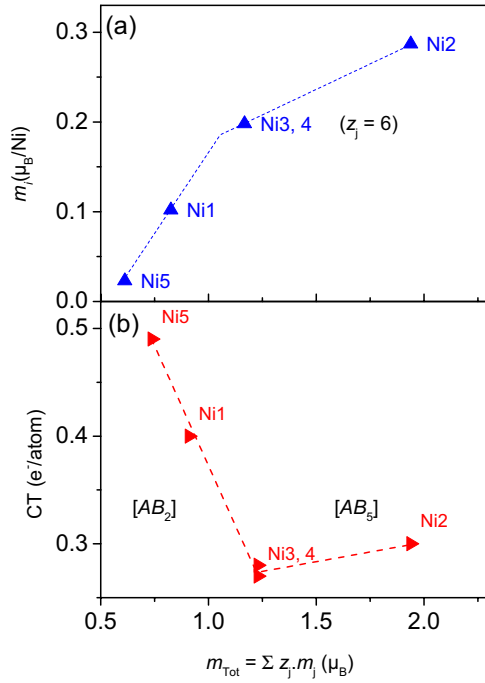


Figure 6. Ni moment and charge transfer CT from La to Ni versus the sum of the Ni moments in the first coordination sphere m_{Tot} for each Ni site in $2H\text{-La}_2\text{Ni}_7$.

Ni3 and Ni4 moments. On the other hand the Ni2 atoms are surrounded by 8 Ni at distances between 2.45 and 2.62 Å forming a more regular polyhedron with 4 Ni2 neighbors in the basal plane and 4 Ni3 (Ni4) neighbors in the equatorial plane. The Ni1 atoms are surrounded by 4 Ni1 in the basal plane, 1 Ni5, 1 Ni3 and 1 Ni4 with distances ranging between 2.45 Å and 2.62 Å. The Ni5 atoms are surrounded by 6 Ni1 atoms at 2.55 Å (figure 5(right)).

In a simple molecular field approximation, the Ni–Ni exchange interactions can be described by an internal field H_{exch} acting on the Ni site and resulting from the closest Ni neighbor moments (the influence of the Ni–La interactions can be neglected as they are much smaller):

$$H_{\text{exch}} = \lambda_{\text{Ni-Ni}} \cdot m_{\text{Tot}} \quad (1)$$

where $\lambda_{\text{Ni-Ni}}$ is the Ni–Ni molecular field coefficient and $m_{\text{Tot}} = \sum_j z_j \cdot m_j$ is the sum of the z_j Ni neighbor moments m_j . Assuming that the Ni–Ni short range interaction is close for all Ni atoms and that the exchange integrals are not very different for the Ni–Ni distances between 2.45 and 2.62 Å, it is possible to verify if there is any proportionality between the Ni moments on each site and the sum of its first neighbor moments. The variation of each Ni moment (m_i) versus m_{Tot} shows two different behaviors for the Ni atoms related to the $[AB_2]$ units and those belonging to the $[AB_5]$ units (figure 6(a)) with a dm_i/dm_{Tot} slope of 0.58 and 0.125 respectively. To explain this difference of behavior, which cannot be only due to the variation of Ni–Ni distances as they are comparable for Ni1 and Ni2 atoms and their next Ni neighbors, one should also consider the influence of the first La neighbors ($2.93 \text{ \AA} \leq d_{\text{Ni-La}} \leq 3.33 \text{ \AA}$).

The electronic charge transfer CT from La to Ni atoms is calculated using the Bader method and is given as a function

of m_{Tot} in figure 6(b). Similar to the m_i individual moments, the CT presents two different behaviors for Ni in $[AB_2]$ and $[AB_5]$ units: a sharp decrease from Ni5 to Ni3,4 and an almost constant CT value for Ni3,4 and Ni2 atoms. The CT values are related to the number of La first neighbors (table 1). For Ni atoms with the largest CT values (Ni5 and Ni1) the additional electrons transferred from La atoms contribute to a progressive filling of the d -Ni bands. It yields a reduction of their local magnetic moment compared to the values extrapolated from Ni3,4 or Ni2 moment versus m_{Tot} .

As a consequence, the magnitude of the Ni moments can be related to their positions relative to the $[AB_2]$ and $[AB_5]$ units. For both structure types, it appears that the Ni moment is maximum for the Ni2 atoms located between two $[AB_5]$ units and minimum for the Ni5 ($2a$) atoms belonging to the $[AB_2]$ units, at the $z = 1/2$ plane containing the center of symmetry of the cell. This is illustrated in figure 7, where the hexagonal structure of La_2Ni_7 and the corresponding magnitude of the Ni moments along the c axis are presented. Similar Ni moment distribution can be obtained for $3R\text{-Y}_2\text{Ni}_7$. It is also noticeable that the distribution of Ni magnetic moments along half the hexagonal cell forms a triangle. This is repeated twice, because the stacking $[A_2B_4 + 2 AB_5]$ is repeated two times in this hexagonal lattice, whereas the same sequence appears three times in $3R\text{-Y}_2\text{Ni}_7$. This emphasizes a kind of modulation of the Ni moments along the c -axis.

The dependence of the Ni magnetic moments versus their localization in $[AB_2]$ and $[AB_5]$ units in hexagonal La_2Ni_7 can be partly related to the difference of magnetic properties of the corresponding binary LaNi_2 and LaNi_5 compounds: LaNi_2 is a Pauli paramagnet with a weak susceptibility ($\chi = 1.5 \cdot 10^{-4}$ emu/mole) [33] whereas LaNi_5 is an enhanced Pauli paramagnet with $\chi = 2.0 \cdot 10^{-3}$ emu/mole [50]. In general, ANi_5 compounds are close to the onset of ferromagnetism, but the $N(E_F)$ is not large enough to stabilize a ferromagnetic state. The weak itinerant magnetism observed in $A_2\text{Ni}_7$ as well as ANi_3 compounds has been attributed to the existence of the sharp and narrow peak near E_F providing a large enough $N(E_F)$ contribution to stabilize a SP state [51].

However, all the experimental studies have shown that the magnetic ground state of $2H\text{-La}_2\text{Ni}_7$ is characteristic of an AFM structure ($T_N = 50 \text{ K}$). In addition, $2H\text{-La}_2\text{Ni}_7$ undergoes a metamagnetic transition towards a FM state with a transition field of 4.6 T and a stabilization of a wFM behavior above 6 T at 4.2 K [27]. Up to now, all the studies performed on La_2Ni_7 did not allow to propose an AFM structure filling these criteria. The only observation obtained from the DOS calculation was the smaller $N(E_F)$ value of La_2Ni_7 compared to Y_2Ni_7 [46].

Taking into account the symmetry of the hexagonal structure (2 blocks of $[AB_2 + 2 AB_5]$) and assuming that the Ni5 moments, which belong to the $[AB_2]$ unit and are already very small in the calculated FM structure ($m_{\text{Ni5}} = 0.023 \mu_B/\text{Ni}$) are equal to zero, the AFM structure presented in figure 7 can be proposed. The spins of the Ni atoms are of same sign in the same block (between layers at $z = 0$ and $1/2$) whereas they have opposite sign in the next stacking (between $z = 1/2$ and 1), and they are all aligned parallel to the c axis. In other words, Ni atoms in the same block are ferromagnetically

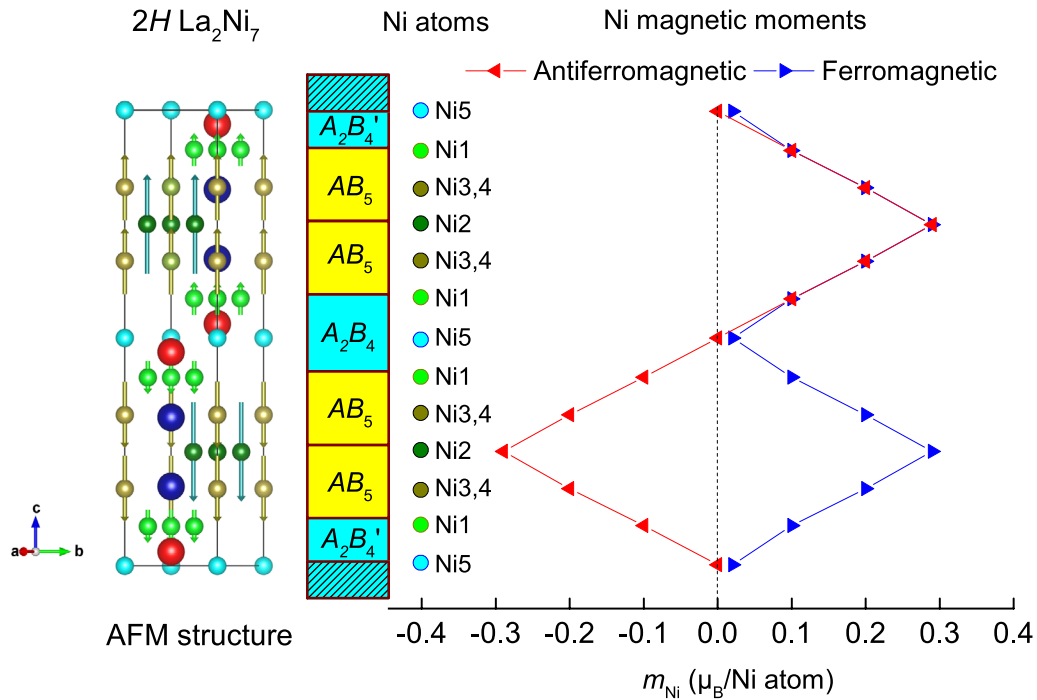


Figure 7. Antiferromagnetic structure of La_2Ni_7 and Ni moment distribution along the c axis in both antiferromagnetic (red) and ferromagnetic (blue) structures of La_2Ni_7 . (Color online).

aligned while the magnetic coupling between adjacent blocks is antiferromagnetic (table 1 and figure 7). The DFT calculation converges to the proposed AFM structure with a net magnetization equal to zero on the Ni5 site and an antiferromagnetic coupling between the Ni1 atoms which are its nearest neighbors and belonging to the different blocks ($z < 1/2$ or $z > 1/2$). Due to the particular point symmetry of the Ni5 site ($\bar{3}m.$), the molecular field generated by the six Ni1 neighbor atoms forming two tetrahedra with antiparallel spin cancels exactly at this $2a$ position (figure 5(left)). This can explain that these Ni5 atoms have no ordered moments in the AFM structure. On the contrary in the FM configuration, where all the Ni moments are parallel to the c axis a small Ni moment is induced on the $2a$ position by the magnetic moments of the 6 Ni1 neighbors as explained above (figure 5(right)).

Similar geometric environment with a central atom surrounded by six neighbors, which can be coupled ferromagnetically or antiferromagnetically, depending on the presence of an ordered moment or not on the central atom position, has been observed in other Laves phase systems: C14 hexagonal TiFe_2 , $\text{Hf}_{0.825}\text{Ta}_{0.175}\text{Fe}_2$ and monoclinic $\text{YFe}_2\text{H}_{4.2}$ derived from a C15 cubic parent compound [52–54].

In La_2Ni_7 , the distance between two next Ni1 neighbors of different blocks connected via a Ni5 atom is 5.20 Å and these distances are large enough to favor negative $J_{\text{Ni1-Ni1}}$ interactions in the absence of a moment on Ni5 site. Except for Ni5 atoms, all the other Ni atoms carry Ni moments whose magnitudes are close to those calculated in the wFM state (table 1 and figure 4). As their environment remains similar in both FM and AFM structures, they are less affected by the magnetic ordering contrary to the Ni5 atoms.

The DOS for this AFM structure shows that the narrow peak observed in NSP DOS is shifted below E_F for the majority spin and $N(E_F)$ falls in a valley at E_F (figure 3(c)). However, only from the energy calculated for the proposed AFM and the FM structures, it is not possible to distinguish the most stable state since the difference is negligible with less of 1 meV/at., whereas the DFT accuracy is known to be few meV/at.. Thus, whatever the XC functional or method, the DFT calculation indicates that both magnetic structures present the same stability at 0K. In table 2, the total energy difference of A_2Ni_7 compounds is compared in NSP, FM and AFM structures for both the rhombohedral and hexagonal symmetries. It shows that the most stable state is the magnetic state (AFM or FM) for both La_2Ni_7 and Y_2Ni_7 without a clear difference between both symmetries, as already discussed in previous paper about stacking phases [34].

The DFT calculation allows to propose an hexagonal AFM structure, whereas it become more challenging to propose an AFM structure for the rhombohedral cell. In fact, the AFM ordering requires an even number of blocks to cancel the total magnetic moment, as observed in the Ce_2Ni_7 type structure. As the Gd_2Co_7 type structure contains three blocks, it will require a doubling of the unit cell along the c axis to obtain a comparable AFM order. As the c parameter of $3R\text{-Y}_2\text{Ni}_7$ is already 36.19 Å, this will generate a very anisotropic magnetic cell with $cla \approx 15$, compared to only $cla \approx 5$ for $2H\text{-La}_2\text{Ni}_7$. Although we have not calculated such large magnetic cell, it was observed experimentally that $3R\text{-La}_2\text{Ni}_7$ should have a ferromagnetic ground state. Indeed, the magnetization curves of La_2Ni_7 sample annealed at 873 K and containing a mixture of hexagonal and rhombohedral phases, were analyzed by a superposition of FM and AFM states [27].

Table 2. Heat of formation of A_2Ni_7 compounds in both allotropic hexagonal and rhombohedral structures in different magnetic states. For hexagonal La_2Ni_7 the calculations were done with different functionals and method as described in the text.

Compound	XC- method	Structure	Magnetic state	$\Delta E = E(i) - E(NSP)$ (meV/f.u.)
Y_2Ni_7	GGA	Rhombohedral	NSP	0
			FM	-35
		Hexagonal	NSP	0
			FM	-35
			AFM	-33
La_2Ni_7	GGA	Rhombohedral	NSP	0
			FM	-31
		Hexagonal	NSP	0
			FM	-35
			AFM	-33
	Non-colinear	M parallel to z	FM	-34
			AFM	-33
	Non-colinear	M parallel to x, y	FM	-3
			LDA	Hexagonal
	LDA	Hexagonal	FM	-22
			AFM	-20
			SCAN	Hexagonal
	SCAN	Hexagonal	FM	-75
			AFM	-72
			GGA + U	Hexagonal
GGA + U	Hexagonal	FM	-35	
		AFM	-32	

This proposed AFM structure for $2H-La_2Ni_7$ allows explaining several experimental features of the literature as detailed below:

- (i) it confirms the high uniaxial anisotropy determined from the magnetization curves of $2H-La_2Ni_7$ by Parker *et al* [27]. They calculated an anisotropy field of at least 12 T and an uniaxial anisotropy energy greater than 160 kJ m^{-3} .
- (ii) It can explain the positive value of θ_P above T_N [26, 27, 30, 33], as locally the FM interactions remain larger than the AFM ones. Parker *et al* [27], already suggested that the large value of θ_P was characteristic of a metamagnetic behavior of a compound which has uniaxial anisotropy and with ferromagnetic intralayer and antiferromagnetic interlayer exchange interactions.
- (iii) The study of $2H-La_2Ni_7$ by NPD did not allow to observe magnetic lines at low temperature [33]. A simulation of the NPD pattern was therefore done for FM and AFM structures assuming a wavelength of 2.43 \AA , typical of a spectrometer dedicated for magnetic structure determination (figure S2). This reveals how it will be difficult to observe the magnetic structures experimentally. As the magnetic cell has a $[000]$ propagation vector, it would only increase very weakly few nuclear line intensities. The most intense AFM magnetic line will contribute to only 1.2% of the (100) Bragg peak and even less considering the experimental moments and not the calculated one.

Although the DFT calculations cannot observe a clear difference of stability between the AFM and FM structures, all

the experimental magnetic studies clearly indicates that the ground state of $2H-La_2Ni_7$ is AFM. But the difference of stability between the two types of magnetic order is clearly small: it was observed experimentally that the substitution of only 3 at% of Cu for Ni stabilizes a FM state, whereas the AFM ground state is maintained up to 10 at% Co [29]. This difference was attributed to a critical number of d electrons as the total number of d -electron increases upon Cu substitution and decreases upon Co substitution. It confirms that we are very close to the limit of stability of the AFM structure, which can be favored by the existence of spin-fluctuations. The low value of the saturation moment and the large Rhodes-Wohlfarth ratio observed for both $2H-La_2Ni_7$ [27, 29, 30, 33] and $3R-Y_2Ni_7$ compounds [25] as well as other experimental results confirms their weak itinerant character and the existence of large spin fluctuations in both compounds. In addition, the metamagnetic behavior of the magnetization curves of La_2Ni_7 was analyzed within the Moriya and Usami theory using a Landau-type free energy equation, used in the frame of systems with large spin fluctuations [30, 55, 56].

For weak itinerant magnetic systems, the existence of large spin fluctuations was able to explain the difference between results obtained by DFT calculations and those observed experimentally. For example, Ni_3Ga is a strongly renormalized paramagnet, but the DFT calculation predicts a weak ferromagnetic ground state similar to isostructural Ni_3Al , with even larger Ni moment [9]. This difference has been explained by taking into account the low-frequency spin fluctuations present in this compound which is close to a ferromagnetic quantum critical point. The theoretical study of

TiAu confirmed also the influence of spin fluctuations for the stabilization of the weak antiferromagnetic state, as well as the overestimation of the Ti moment determined by DFT calculations [19]. Such overestimation of magnetic moment is often observed for compounds which lies close to quantum critical point.

In the case of $2H\text{-La}_2\text{Ni}_7$ the magnetic order is driven by the magnitude of the Ni5 moment which is predicted by DFT calculation to be $0.023 \mu_B$ in the FM structure and 0 in the AFM structure. But it was found, that the total magnetic moment of $2H\text{-La}_2\text{Ni}_7$ in FM state is overestimated of at least 30% compared to the experimental value. In this case, the influence of spin fluctuations on the particular Ni5 site should be large enough to stabilize a geometric environment with the next Ni1 neighbors adopting an antiparallel coupling.

4. Conclusions

In this work, we have proposed for hexagonal La_2Ni_7 an AFM structure with a stability comparable to that of the FM structure. This AFM structure of $2H\text{-La}_2\text{Ni}_7$ results from the geometric conditions presented by its stacked hexagonal structure: the molecular field is canceled on the Ni5-2a site at $z = 0$ and $z = 1/2$ which belong to the $[AB_2]$ units and acts as an inversion center for the first neighbors Ni at the interface between the $[AB_2]$ and $[AB_5]$ units (Ni1-12k). These nearest Ni atoms adopt an AFM coupling and the symmetry of the structure on this position allows an inversion of the sign of the other Ni spin orientation belonging to different blocks. This generates a modulated AFM structure with two ferromagnetic slabs of opposite directions separated by a non-magnetic layer. Such magnetic structure type was already observed in some AFe_2 Laves phases or their hydrides. The metamagnetic transition from AFM towards a FM structure is explained by a non-zero Ni moment on the Ni5 site induced by the application of a magnetic field.

The stabilization of this AFM structure, observed experimentally, should be explained by the existence of large spin fluctuations, not taken into account by simple DFT calculation, as observed for other weak itinerant magnets as Ni_3Ga or TiAu. Further works using Moriya and Usami theory of spin fluctuation, could be very interesting to consider for La_2Ni_7 .

Further experimental and theoretical studies will be performed on pseudo-binary $\text{La}_{2-x}\text{Y}_x\text{Ni}_7$ compounds to observe the evolution from wAFM $2H\text{-La}_2\text{Ni}_7$ towards wFM $3R\text{-Y}_2\text{Ni}_7$, and verify what the critical geometric and electronic parameters are. First principles calculations of other compounds with stacking structures like ANi_3 or A_5Ni_{19} compounds from $[\text{A}_2\text{Ni}_4 + n \cdot \text{ANi}_5]$ with $n = 1$ and 3 respectively, could be also very interesting in order to analyze the relation between their crystal structures and magnetic properties.

Acknowledgments

The authors are very thankful to M Gupta for her advice and fruitful discussion. DFT calculations were performed using HPC resources from GENCI-CINES (Grant 2019-96175).

ORCID iDs

J-C Crivello  <https://orcid.org/0000-0002-4849-2556>

V Paul-Boncour  <https://orcid.org/0000-0002-0601-7802>

References

- [1] Moriya T, Takahashi Y and Ueda K 1992 Antiferromagnetic spin fluctuations and superconductivity in high-Tc oxides *J. Magn. Magn. Mater.* **104** 456–60
- [2] Ishigaki A and Moriya T 1998 On the theory of spin fluctuations around the magnetic instabilities—effects of zero-point fluctuations *J. Phys. Soc. Japan* **67** 3924–35
- [3] Moriya T R and Ueda K 2003 Antiferromagnetic spin fluctuation and superconductivity *Rep. Prog. Phys.* **66** 1299–341
- [4] Mazin I I and Singh D J 2004 Spin fluctuations and the magnetic phase diagram of ZrZn_2 *Phys. Rev. B* **69** 020402
- [5] Kabeya N, Maekawa H, Deguchi K, Kimura N, Aoki H and Sato N K 2013 Phase diagram of the itinerant-electron ferromagnet ZrZn_2 *Phys. Status Solidi b* **250** 654–56
- [6] Morkowski J A and Wosicki P 1992 Theory of magnetic and thermal-properties of the weak itinerant ferromagnet Ni_3Al *J. Magn. Magn. Mater.* **104** 673–74
- [7] Guo G Y, Wang Y K and Hsu L S 2002 First-principles and experimental studies of the electronic structures and magnetism in Ni_3Al , Ni_3Ga and Ni_3In *J. Magn. Magn. Mater.* **239** 91–3
- [8] Steiner M J, Beckers F, Niklowitz P G and Lonzarich G G 2003 Non-Fermi liquid form of the low temperature resistivity in the low moment ferromagnets Ni_3Al and YNi_3 *Physica B* **329** 1079–80
- [9] Aguayo A, Mazin I I and Singh D J 2004 Why Ni_3Al is an itinerant ferromagnet but Ni_3Ga is not *Phys. Rev. Lett.* **92** 147201
- [10] Velasco V, Crespo P, Marín P, García-Escorial A, Lieblich M, González-Calbet J M, Ynduráin F and Hernando A 2015 Short range order fluctuations and itinerant ferromagnetism in Ni_3Al *Solid State Commun.* **201** 111–4
- [11] Chen G M, Lin M X and Ling J W 1994 Spin fluctuation effect in the ordered Fe_2N alloy *J. Appl. Phys.* **75** 6293–5
- [12] Naganuma H, Endo Y, Nakatani R, Kawamura Y and Yamamoto M 2004 Magnetic properties of weak itinerant ferromagnetic $\zeta\text{-Fe}_2\text{N}$ film *Sci. Technol. Adv. Mater.* **5** 83–7
- [13] Lin S, Lv H Y, Lin J C, Huang Y A, Zhang L, Song W H, Tong P, Lu W J and Sun Y P 2018 Critical behavior in the itinerant ferromagnet AsNCr_3 with trigonal-antiperovskite structure *Phys. Rev. B* **98** 014412
- [14] Matthias B T, Giorgi A L, Struebing V O and Smith J L 1978 Itinerant antiferromagnetism of TiBe_2 *Phys. Lett. A* **69** 221
- [15] Povzner A A and Likhachev D V 1995 Spin fluctuation theory for temperature-induced ferromagnetism in itinerant antiferromagnets and paramagnets *Int. J. Mod. Phys. B* **9** 1171–84
- [16] Torun E, Janner A and de Groot R A 2016 Origin of weak magnetism in compounds with cubic Laves structure *J. Phys.: Condens. Matter* **28** 065501
- [17] Svanidze E *et al* 2015 An itinerant antiferromagnetic metal without magnetic constituents *Nat. Commun.* **6** 7701
- [18] Goh W F and Pickett W E 2016 A mechanism for weak itinerant antiferromagnetism: mirrored van Hove singularities *Europhys. Lett.* **116** 27004
- [19] Goh W F and Pickett W E 2017 Competing magnetic instabilities in the weak itinerant antiferromagnetic TiAu *Phys. Rev. B* **95** 205124

- [20] Mathew M, Fong Goh W and Pickett W E 2019 Probing hole-doping of the weak antiferromagnet TiAu with first principles methods *J. Phys.: Condens. Matter* **31** 074005
- [21] Solontsov A Z and Silin V P 2004 Weak itinerant-electron antiferromagnetism of uranium nitride *Phys. Met. Metallogr.* **97** 571–81
- [22] Singh D J 2015 Electronic structure and weak itinerant magnetism in metallic Y_2Ni_7 *Phys. Rev. B* **92** 174403
- [23] Buschow K H J 1984 Magnetic-properties of Y_2Ni_7 and its hydride *J. Less-Common Met.* **97** 185–90
- [24] Tolkachev O M 1990 Spin fluctuation mechanism for the temperature-induced magnetic moment (TIMM) in the electron liquid of Y_2Ni_7 Alloy *Phys. Status Solidi b* **159** K115–8
- [25] Bhattacharyya A, Jain D, Ganesan V, Giri S and Majumdar S 2011 Investigation of weak itinerant ferromagnetism and critical behavior of Y_2Ni_7 *Phys. Rev. B* **84** 184414
- [26] Buschow K H J 1983 Magnetic properties of La_2Ni_7 and its hydride *J. Magn. Magn. Mater.* **40** 224–6
- [27] Parker F T and Oesterreicher H 1983 Magnetic properties of La_2Ni_7 *J. Less-Common Met.* **90** 127–36
- [28] Fukase M, Tazuke Y, Mitamura H, Goto T and Sato T 1999 Successive metamagnetic transitions in hexagonal La_2Ni_7 *J. Phys. Soc. Japan* **68** 1460–1
- [29] Fukase M, Tazuke Y, Mitamura H, Goto T and Sato T 2000 Itinerant electron magnetism of hexagonal La_2Ni_7 *Mater. Trans.* **41** 1046–51
- [30] Tazuke Y, Suzuki H and Tanikawa H 2004 Metamagnetic transitions in hexagonal La_2Ni_7 *Physica B* **346** 122–6
- [31] Nakabayashi R, Tazuke Y and Murayama S 1992 Itinerant Electron Weak Ferromagnetism in Y_2Ni_7 and YNi_3 *J. Phys. Soc. Japan* **61** 774–7
- [32] Tazuke Y, Nakabayashi R, Murayama S, Sakakibara T and Goto T 1993 Magnetism of R_2Ni_7 and RNi_3 ($R = Y, La, Ce$) *Physica B* **186–8** 596–8
- [33] Tazuke Y, Abe M and Funahashi S 1997 Magnetic properties of La–Ni system *Physica B* **237–8** 559–60
- [34] Crivello J C, Zhang J and Latroche M 2011 Structural stability of AB(y) phases in the (La,Mg)–Ni system obtained by density functional theory calculations *J. Phys. Chem. C* **115** 25470–8
- [35] Kresse G and Hafner J 1993 *Ab initio* molecular dynamics for open-shell transition metals *Phys. Rev. B* **48** 13115
- [36] Kresse G and Joubert D 1999 From ultrasoft pseudopotentials to the projector augmented-wave method *Phys. Rev. B* **59** 1758
- [37] Blöchl P E 1994 Projector augmented-wave method *Phys. Rev. B* **50** 17953–79
- [38] Perdew J P and Zunger A 1981 Self-interaction correction to density-functional approximations for many-electron systems *Phys. Rev. B* **23** 5048–79
- [39] Perdew J P, Burke K and Ernzerhof M 1996 Generalized gradient approximation made simple *Phys. Rev. Lett.* **77** 3865–8
- [40] Perdew J P, Burke K and Ernzerhof M 1997 Generalized gradient approximation made simple *Phys. Rev. Lett.* **78** 1396
- [41] Sun J, Ruzsinszky A and Perdew J P 2015 Strongly constrained and appropriately normed semilocal density functional *Phys. Rev. Lett.* **115** 036402
- [42] Rohrbach A, Hafner J and Kresse G 2003 Electronic correlation effects in transition-metal sulfides *J. Phys.: Condens. Matter* **15** 979–96
- [43] Blöchl P E, Jepsen O and Andersen O K 1994 Improved tetrahedron method for Brillouin-zone integrations *Phys. Rev. B* **49** 16223
- [44] Bader R 1990 *Atoms in Molecules. A Quantum Theory* (Oxford: Clarendon)
- [45] Henkelman G, Arnaldsson A and Jónsson H A 2006 Fast and robust algorithm for Bader decomposition of charge density *Comput. Mater. Sci.* **36** 354–60
- [46] Werwinski M, Szajek A, Marczyńska A, Smardz L, Nowak M and Jurczyk M 2018 Effect of substitution La by Mg on electrochemical and electronic properties in $La_{2-x}Mg_xNi_7$ alloys: a combined experimental and *ab initio* studies *J. Alloys Compd.* **763** 951–9
- [47] Werwiński M, Szajek A, Marczyńska A, Smardz L, Nowak M and Jurczyk M 2019 Effect of Gd and Co content on electrochemical and electronic properties of $La_{1.5}Mg_{0.5}Ni_7$ alloys: a combined experimental and first-principles study *J. Alloys Compd.* **773** 131–9
- [48] Quan Y and Pickett W E 2016 Van Hove singularities and spectral smearing in high-temperature superconducting H_3S *Phys. Rev. B* **93** 104526
- [49] Stoner E C 1939 Collective electron ferromagnetism II. Energy and specific heat *Proc. R. Soc. A* **169** 339–71
- [50] Gignoux D, Givord F, Lemaire R and Tasset F 1983 Onset of ferromagnetism and spin fluctuations in rare earth (or actinide)-3d compounds *J. Less-Common Met.* **94** 1–15
- [51] Shimizu M, Inoue J and Nagasawa S 1984 Electronic-structure and magnetic-properties of Y–Ni intermetallic compounds *J. Phys. F Met. Phys.* **14** 2673–87
- [52] Brown P J, Deportes J and Ouladdiaf B 1992 Magnetic structure of the Laves phase compound $TiFe_2$ *J. Phys.: Condens. Matter* **4** 10015–24
- [53] Diop L V B, Isnard O, Suard E and Benea D 2016 Neutron diffraction study of the itinerant-electron metamagnetic $Hf_{0.825}Ta_{0.175}Fe_2$ compound *Solid State Commun.* **229** 16–21
- [54] Paul-Boncour V, Guillot M, Isnard O, Ouladdiaf B, Hoser A, Hansen T and Stuesser N 2017 Interplay between crystal and magnetic structures in $YFe_2(H_αD_{1-α})_{4.2}$ compounds studied by neutron diffraction *J. Solid State Chem.* **245** 98–109
- [55] Moriya T 1979 Recent progress in the theory of itinerant electron magnetism *J. Magn. Magn. Mater.* **14** 1–46
- [56] Moriya T 1991 Theory of itinerant electron magnetism *J. Magn. Magn. Mater.* **100** 261–71